THE ASTROPHYSICAL JOURNAL, 369:314–319, 1991 March 10

THE NUMBER COUNT DISTRIBUTION FOR X-RAY–SELECTED BL LACERTAE OBJECTS AND CONSTRAINTS ON THE LUMINOSITY FUNCTION[1]

ANNA WOLTER,[2] I. M. GIOIA,[2,3] T. MACCACARO,[2,4] S. L. MORRIS,[5] AND J. T. STOCKE[6]

Received 1990 February 26; accepted 1990 August 23

ABSTRACT

In this paper we describe a sample of 34 BL Lac objects extracted from the *Einstein* Extended Medium Sensitivity Survey. X-ray selection has proved to be a powerful way to find new BL Lac objects and to generate complete and well-defined samples. We compute the number-count relationship and compare it with the results of other X-ray surveys. Then, we assume different models of the intrinsic X-ray luminosity function and study the effect of beamed X-ray emission on the resulting observed luminosity function, comparing the predicted number-count distribution with the observed one. Using the available redshift information, we can exclude that the AGN X-ray luminosity function (we include in the class of AGN all emission-line objects, like quasars and Seyfert galaxies), modified by beaming, can describe that of BL Lac objects, even though the predicted log N–log S relationship is in agreement with the observations.

Subject headings: BL Lacertae objects — galaxies: nuclei — galaxies: X-rays

1. INTRODUCTION

Sizable samples of BL Lac objects can be constructed using X-ray surveys. In fact, the number of BL Lacs found in recent years by means of their X-ray emission is comparable to the total number of BL Lac objects ever found by all other means combined. There are currently 34 BL Lac objects in the *Einstein* Extended Medium Sensitivity Survey (two more than in Stocke et al. 1990a), 11 in the High Galactic Latitude survey by the *EXOSAT Observatory*, 23 in the *HEAO 1* A-1 + A-3 all sky-survey (which is currently ~65% identified), and five from the *HEAO 1* A-2 experiment. This compares with the 79 BL Lac objects from the Hewitt and Burbidge catalog (1987) which are not X-ray–selected. The number of X-ray–selected BL Lac objects is still small if compared with the number of AGNs (3594 from the Hewitt and Burbidge catalog), but the completeness of the samples makes them worthy of interest for statistical studies and derivation of the properties of the class.

We present here the sample of BL Lac objects extracted from the Extended Medium Sensitivity Survey (§ 2), and then derive their number count distribution (§ 3). In § 4 we discuss the implications on the X-ray luminosity function of BL Lac objects. The present work represents a significant update over similar results presented elsewhere (Maccacaro et al. 1984a, 1989). A Friedmann universe with a deceleration parameter $q_0 = 0$ and a Hubble constant $H_0 = 50$ are used to compute volumes and luminosities.

2. THE SAMPLE AND ITS PROPERTIES

We adopt here the definition of BL Lac objects proposed by Stocke et al. (1990a). We recall for the sake of completeness the observational properties we use to classify an X-ray source as a BL Lac object. The classification is based on the optical spectrum, mainly taken in the range 3400–6400 Å, with a resolution of typically 7–8 Å. We impose upper limits on the featurelessness of the optical spectrum, in the sense that no emission lines should be present with $W_\lambda \geq 5$ Å. If a Ca II H and K break is present, due to starlight from the underlying galaxy, then it must have a contrast $\leq 25\%$ (Stocke et al. 1988). We do not put any requirement on the radio emission, so as to not bias *a priori* against the possibility of finding radio-quiet BL Lac objects (see below and the discussion in Stocke et al. 1990a). This definition of BL Lac object keeps them clearly separated from the class of AGN, where we include quasars and Seyfert galaxies. Furthermore, the overall spectral properties of the two classes of AGNs and BL Lac objects are different, as shown in Figure 1.

Thirty-four of the X-ray sources in the *Einstein* Extended Medium Sensitivity Survey (EMSS) satisfy the above criteria for identification as a BL Lac object. The EMSS is described in detail in Gioia et al. (1990). The EMSS is a sample of serendipitous X-ray sources, detected with the IPC on board the *Einstein* Observatory. The sample is statistically complete and well defined. The survey covers an area of about 780 deg^2 (~3%) of the high Galactic latitude sky, at a sensitivity level that ranges between 5×10^{-14} and 3×10^{-12} ergs cm^{-2} s^{-1} in the 0.3–3.5 keV band. The fluxes of the sources detected span between 6×10^{-14} and $\sim 10^{-11}$ ergs cm^{-2} s^{-1}. All the fluxes are computed assuming a power-law spectrum with energy index $\alpha = 1.0$, and absorption due to the Galactic hydrogen column toward the source as measured by the 21 cm observations by Stark et al. (1984). The optical program of spectroscopic identification is near completion (Stocke et al. 1990b). As of 1990 May, we have identified 95.5% of the sample (797 sources out of 835).

The fact that the sample is not 100% identified might imply that the results are subject to some degree of uncertainty. We want to show that the present uncertainties are, however, not likely to significantly affect the conclusions of this paper. The identification process started from the sources at higher fluxes; only two sources at X-ray fluxes higher than 5×10^{-13} ergs cm^{-2} s^{-1} remain without a positive identification. Moreover,

[1] This paper uses data obtained at the Multiple Mirror Telescope Observatory (MMTO), which is operated jointly by the University of Arizona and the Smithsonian Institution.

[2] Harvard-Smithsonian Center for Astrophysics, 60 Garden Street, Cambridge, MA 02138.

[3] Also at Istituto di Radioastronomia del CNR, Bologna, Italy.

[4] Also at Osservatorio Astronomico di Bologna, Italy.

[5] The Observatories of the Carnegie Institute of Washington, 813 Santa Barbara Street, Pasadena, CA 91101.

[6] Center for Astrophysics and Space Astronomy, University of Colorado, Campus Box 391, CO 80309.

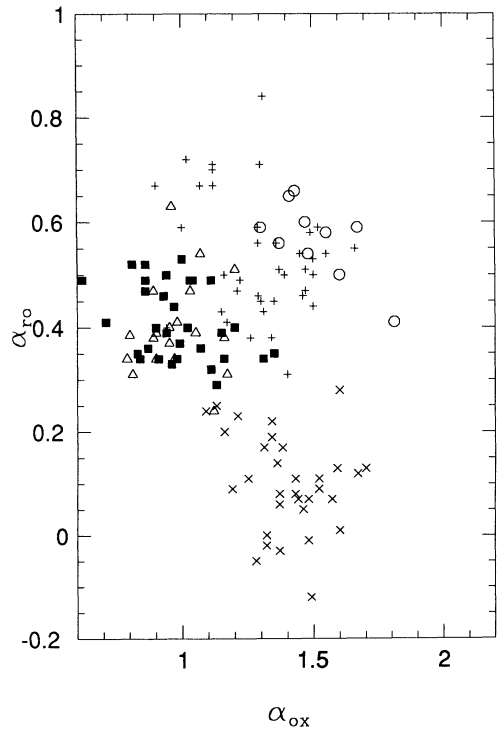

FIG. 1.—The α_{ro} vs. α_{ox} diagram for various classes of extragalactic objects. Squares are X-ray–selected BL Lac objects from the EMSS; circles are radio-selected BL Lac objects; plus signs are X-ray–selected radio-loud AGNs; crosses are X-ray–selected radio-quiet AGNs; triangles are BL Lac objects from the *HEAO 1* A-1–A-3 experiments, both radio- and X-ray–selected. X-ray fluxes have been recomputed with respect to the similar diagram presented in Stocke et al. (1990), using the new detection algorithm (Rev. 1) and an appropriate choice for the spectral parameters (see Gioia et al. 1990 for details).

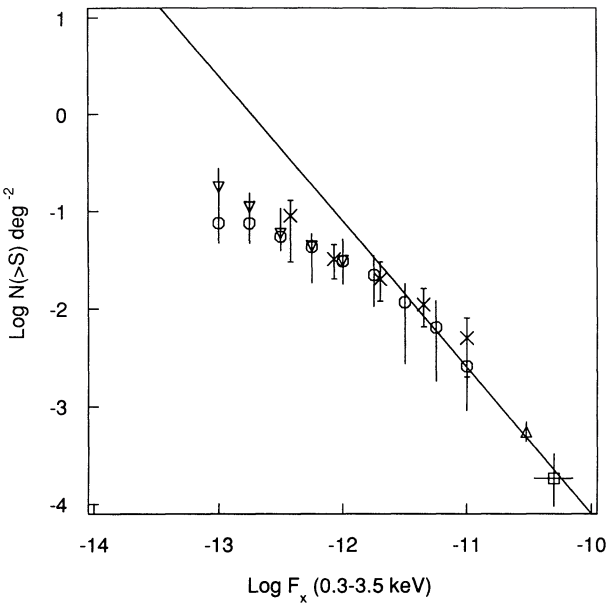

FIG. 2.—The X-ray surface density of BL Lac objects. The open square is from the *HEAO 1* A-2 survey by Piccinotti et al (1982). The open circles are the EMSS BL Lac objects; the downward-pointing triangles represent the maximum variation in density possible for EMSS BL Lac objects (see text for details). The triangle is from the *HEAO"1* A-1–A-3 experiments (Schwartz et al. 1989b). The crosses are from the *EXOSAT* High Galactic Latitude survey by Giommi et al. (1989) using a spectral index $\alpha = 1.5$. The error bars represent Poisson statistical errors. The solid line indicates the Euclidean slope normalized to the counts at higher fluxes.

we can exclude the presence of a significant number of BL Lac objects among the still unidentified sources at all fluxes. If we follow the conclusion of Stocke et al. 1990a (based on a completely identified subsample of the EMSS) that no class of radio-quiet BL Lac objects exists, then BL Lac objects can only be found among the unidentified EMSS sources that are also radio sources. There are two such sources, and there are 12 unidentified objects that have no radio observations. Out of 617 EMSS objects observed in the radio, 169 are radio emitters. We assume that the same detection ratio applies for these 12 sources not yet observed in the radio, since the lack of radio information is usually due to the fact that the sources were not visible at the time of the observation or below the declination range of the telescope. Hence, the total number of radio-emitting unidentified sources is probably ≤ 5.3. Since only a fraction of these are likely to be BL Lac objects, we conclude that the number of BL Lac objects still to be found in the survey is small. Consequently, we are confident that the results presented here will not be affected significantly by the identification of the remaining EMSS sources. The number of possible BL Lac objects, together with their flux distribution, will be used in § 3 to derive upper limits to the density of BL Lac objects (Fig. 2).

We used the NRAO Very Large Array[7] at 6 cm, mostly in the C configuration (snapshot mode) to observe the 33 EMSS BL Lac objects that have $\delta > -42°$. A sensitivity of ~ 0.2 mJy (1 σ) is achieved in about 5 minutes of integration. *All* the observed objects have been detected at radio fluxes greater than 1 mJy. For the 10 brightest BL Lac objects, we also have multifrequency observations at 20–18, 6, and 2 cm. Analysis of these data is in progress and will be published elsewhere.

Two new objects are included in the sample with respect to Stocke et al (1990a). They are MS 0331.3−3629, with an X-ray flux $f_x = 6.7 \times 10^{-13}$ ergs cm^{-2} s^{-1}, and MS 0958.9+2102, with $f_x = 2.01 \times 10^{-13}$ ergs cm^{-2} s^{-1}.

The overall spectral properties of EMSS BL Lac objects are comparable to those of other X-ray–selected BL Lac objects. Differences can be seen by comparing their spectral properties to those of other classes of objects, such as the EMSS AGN. Using the revised fluxes as described in Gioia et al. (1990) we update in Figure 1 the figure presented in Stocke et al. (1990a) where the radio-to-optical spectral index $[\alpha_{ro} = \log (S_{5\,GHz}/S_{2500\,Å})/5.38]$ is plotted versus the optical–to–X-ray spectral index $[\alpha_{ox} = -\log (S_{2\,keV}/S_{2500\,Å})/2.605]$ for the EMSS BL Lac objects (*filled squares*) and AGN (*pluses* for radio-loud and *crosses* for radio-quiet). BL Lac objects have a restricted range of values in α_{ro} ($0.30 \leq \alpha_{ro} \leq 0.55$). Values in the same range have been found in other X-ray surveys, e.g., the *EXOSAT* "High Galactic Latitude" survey (Giommi et al. 1989), and the *HEAO 1* A-1–A-3 all-sky survey (Schwartz et al. 1989a). Data points from the *HEAO 1* experiments (Schwartz et al. 1989a; *triangles*) and for representative radio-selected BL Lac objects (*circles*) are also added.

3. THE SURFACE DENSITY

The log N–log S relationship of a complete sample of objects is traditionally the first step in the study of general properties

[7] The VLA of the National Radio Astronomy Observatory (NRAO) is operated by Associated Universities, Inc. under contract with the National Science Foundation (NSF).

of the class. Only the information about the flux of each source and the limiting sensitivity of the survey is needed. The sky coverage of the EMSS is a function of flux and spectral shape (see Gioia et al. 1990). The sky coverage published therein is the one appropriate for a class of sources characterized by a power-law spectrum with energy index $\alpha = 1$; thus, it can be used for this BL Lac object sample. We fold it with the flux of each source to get the number count relationship. The EMSS log $N(>S)$–log S was preliminarily presented in Maccacaro et al. (1989), when only 704 sources (84%) were identified. Here we can extend the analysis with confidence to a larger number of objects and to lower fluxes, since the number of identifications has increased to >95.5%. The resulting log $N(>S)$–log S is presented in Figure 2 (*circles*) as a binned integral distribution. The error bars represent Poisson statistical errors, computed according to the differential number of objects in each bin. The downward-pointing triangles above the EMSS points represent the maximum density of BL Lac objects computed assuming the extreme hypothesis that *all* of the unidentified radio sources in the EMSS are indeed BL Lac objects.

The BL Lac objects log $N(>S)$–log S can be further constrained by information from other X-ray surveys. At high fluxes, the surface density from the survey of Piccinotti et al. (1982; *HEAO 1* A-2), and Schwartz et al. (1989b; *HEAO 1* A-1 + A-3) are represented by a square and a triangle, respectively. The crosses are from the High Galactic Latitude survey of Giommi et al. (1989; *EXOSAT* LE).

The *EXOSAT* data are in very good agreement with the EMSS data, and the points at high fluxes fall on the extrapolation of a power-law fit to the brightest EMSS sources. There is a good agreement in the high flux region between the number-counts of X-ray–selected BL Lac objects, as measured with different instruments, both imaging and nonimaging. To compare them with the EMSS BL Lac objects, we need, however, to correct the fluxes for the different bandwidth and responses of the various instruments. The resulting uncertainties, that depend in the first place on the assumed shape of the spectrum in the different flux ranges, prompted us not to use data from different instruments in the global fit of the number counts. A power law with slope 1.5, representing the Euclidean slope, is plotted for reference in Figure 2. It is evident from the figure that there is a flattening in the slope of the observed log $N(>S)$–log S at fluxes below $\sim 10^{-12}$ ergs cm^{-2} s^{-1}. This flattening was suggested by Maccacaro et al. (1984a) using a complete sample that contained only four BL Lac objects and later confirmed from the analysis of a larger sample of sources (Maccacaro et al. 1989).

4. MODELS OF THE LUMINOSITY FUNCTION

An optimal way to study the volume density of BL Lacs is to derive directly their luminosity function. In order to do so, however, it is necessary to measure the redshift for all objects, a difficult and time-consuming task for "lineless" spectra. Due to the presence of a greater amount of starlight in the optical spectra of X-ray–selected BL Lac objects (XBL), as compared to radio-selected BL Lac objects (RBL), we were able to measure redshifts for a number of the EMSS BL Lac objects. We have undertaken a project to complete the redshift measurements that is still underway. When complete (Morris et al. 1991), it will be possible to derive directly the BL Lac X-ray luminosity function. We will make use of the available redshift information later in this paper, in the form of a redshift distribution. We are forced to use an alternative approach to study the general distribution and evolution properties of BL Lac objects. We assume a number of models for the X-ray luminosity function (XLF), and then, integrating the XLF over a range of redshifts and luminosities for each model, we obtain a log $N(>S)$–log S relationship to compare with the observed number-counts. For those models that produce number-counts in agreement with the observations, we use the available redshift distribution to discriminate among models and set further constraints.

In Maccacaro et al. (1989), a single power-law XLF with slope $\alpha = 2.0$–2.5 was shown to produce a log N–log S consistent with the data. At that time, a redshift cutoff was suggested by the incomplete redshift distribution, but it was not required by the data. To produce a flattening of the observed counts, alternative models, based on the assumption of beamed emission (see, e.g., Cavaliere, Giallongo, & Vagnetti, 1986) can be used. We investigate here three basic models that introduce beamed emission and see how this affects the intrinsic XLF and the resulting number-counts. The effect of beaming on the observed XLF has been described by Urry & Shafer (1984).

We assume that the intrinsic X-ray luminosity function is represented by a power law of slope β over a range of luminosities, that is $N(L) = K \times L^{-\beta}$. The observed luminosity $L_{\rm obs}$ is enhanced by a beaming factor δ^p ($L_{\rm obs} = \delta^p L$), where $\delta = [\Gamma(1 - \beta \cos \theta)]^{-1}$ is the Doppler factor of the jet, Γ is the Lorentz factor, and θ is the angle between the line of sight and the velocity of the jet. The value of p is 4 if we consider broad-band luminosities in a fixed luminosity range. The probability of observing a luminosity $L_{\rm obs}$, given the intrinsic luminosity L is given by

$$P(L_{\rm obs} \mid L) = 1/(\beta \Gamma p) \times L^{1/p} L_{\rm obs}^{-(p+1)/p}$$

(see Urry & Shafer 1984). The observed XLF is then given by the convolution of the intrinsic luminosity function and the probability distribution. The resulting beamed XLF is a double power law, with the same slope as the intrinsic XLF at high luminosities ($\beta_1 = \beta$), and slope $\beta_2 = (p + 1)/p$ at low luminosities. The break luminosity $L_{\rm br}$ is given by $L_{\rm min} \times (\delta_{\rm max}/\delta_{\rm min})^p$, where $L_{\rm min}$ is the minimum observed luminosity, and $\delta_{\rm max}$ and $\delta_{\rm min}$ correspond to the minimum and maximum angle to the line of sight (θ).

Table 1 summarizes the parameter values for the intrinsic XLF considered and for the limits used in the log N–log S derivation, for the various models. The value of k_2 is computed by continuity in the differential XLF at the break luminosity; k_1 is the normalization required to fit the upper (high fluxes) portion of the log N–log S. The normalization is in units of Mpc^{-3} $L_{44}^{\beta-1}$, where L_{44} is the luminosity in units of 10^{44} ergs s^{-1}.

In the first model (A) we assume that BL Lac objects are a completely separate class, i.e., their LF does not depend on any other LF. The emission is partially isotropic, while a fraction $f = 0.20$ is beamed with a Γ Lorentz factor of 3 (see, e.g., Ghisellini & Maraschi 1989; $\Gamma = 3$–5; Padovani & Urry 1990: $\Gamma = 3.4$). We assume a slope of 2.5 that gives a good fit to the high flux portion of the log N–log S. Since we consider all angles, it follows that $\delta_{\rm max} = 5.83$ and $\delta_{\rm min} = 0.33$ are the beaming factors at the minimum (0°) and maximum (90°) viewing angles. The slopes then become $\beta_1 = 2.5$ at high luminosities and $\beta_2 = 1.25$ at low luminosities. From the limited available redshifts we measure an interval of observed luminosities for BL Lac objects from 1.25×10^{43} to 5×10^{46} ergs s^{-1}. It is conceivable and likely that there are objects with

TABLE 1

PARAMETER VALUES FOR THE XLF MODELS AND LIMITS OF INTEGRATION

Model	L_{min} (ergs s^{-1})	L_{max} (ergs s^{-1})	β_1 k_1 ($Mpc^{-3} L_{44}^{\beta_1 - 1}$)	β_2 k_2 ($Mpc^{-3} L_{44}^{\beta_2 - 1}$)	L_{br}	z_{max}
A1	1.25×10^{43}	5.0×10^{46}	2.5 6.3×10^{-7}	1.25 9.4×10^{-9}	2.9×10^{45}	...
A2	1.25×10^{43}	1.0×10^{48}	2.5 6.3×10^{-7}	1.25 9.4×10^{-9}	2.9×10^{45}	...
A3	1.25×10^{43}	5.0×10^{46}	2.5 6.3×10^{-7}	1.25 9.4×10^{-9}	2.9×10^{45}	1
B1	7.0×10^{40}	5.0×10^{46}	2.1 5.2×10^{-8}	1.25 4.4×10^{-7}	8.0×10^{42}	1
B2	7.0×10^{40}	5.0×10^{46}	2.1 5.2×10^{-8}	1.25 4.4×10^{-7}	8.0×10^{42}	...
C1	8.0×10^{41}	1.0×10^{49}	3.6 3.8×10^{-5}	1.25 5.8×10^{-10}	8.9×10^{44} [a]	3

[a] From 8.9×10^{44} to 4.6×10^{46} $\beta_3 \sim 2.0$ and $k_3 \sim 3 \times 10^{-9}$.

even higher luminosity. We first use these limits for integration of the intrinsic luminosity in calculating the counts. Figure 3*a* shows the fit of the model to the observed number counts (A1, *solid curve*). The upper limit is not critical to the behavior of the XLF and the corresponding log N–log S. This choice has a slight effect on the normalization, which has been selected to fit the highest flux EMSS points. This effect is illustrated in Figure 3*a* by the dashed curve, A2, which is the result of an integration up to 1×10^{48} ergs s^{-1}. The integration is carried out over all redshifts without imposing any *a priori* limit. The effect of introducing a redshift "cutoff" is shown by model A3 (Fig. 3*a*, *dotted curve*) where the integration is stopped at $z_{max} = 1$.

The second model we consider (B) is that described in Padovani & Urry (1990). They assume that the Fanaroff-Riley I (FR I) galaxies are the parent population of BL Lac objects and consequently derive a XLF that flattens below the break luminosity of $L_{br} = 8 \times 10^{42}$ ergs s^{-1}. The total luminosity of the source is due to the sum of an isotropic component, L_u and a jet luminosity $L_j = fL_u$, with $f = 0.13$ (Padovani & Urry 1990). The XLF is integrated between 7×10^{40} and 5×10^{46} ergs s^{-1}, and out to a redshift of 1. The slopes are $\beta_1 = 2.10$ and $\beta_2 = 1.25$ (see Table 1). The log $N(>S)$–log S, recomputed here, is plotted in Figure 3*b* (B1, *solid line*). The effect of introducing this redshift cutoff is shown by comparison with the curve B2 (*dotted*) where we use the same parameters as in B1, but without introducing a cutoff in redshift. The log $N(>S)$–log S is steeper in this case, even if the slope is not significantly affected, in agreement with what is mentioned in Padovani & Urry (1990).

Unifying models have been proposed to explain the various kinds of active galactic nuclei. To investigate the possibility that BL Lac objects belong to the same class as AGN, we consider the AGN XLF (as derived in Maccacaro, Gioia, & Stocke 1984b) and, following Cavaliere et al. (1986), we consider the modifications in the XLF introduced by beamed emission. This model does not include a fraction of unbeamed flux as was done in Cavaliere et al. (1986). The AGN XLF was fitted in Maccacaro et al. (1984b) from 4×10^{43} to 1×10^{46} ergs s^{-1} only. Below 4×10^{43} ergs s^{-1} a flattening of the XLF is apparent. Fitting the low-luminosity portion of the XLF (in Fig. 4 of Maccacaro et al. 1984b), we get a slope of 1.5. The resulting beamed XLF has $\beta_2 = 1.25$ at low luminosities, between 8×10^{41} and 9×10^{44} ergs s^{-1}, an intermediate slope $\beta_3 \sim 2.0$ from 9×10^{44} to 4×10^{46} and $\beta_1 = 3.6$ from 4×10^{46} and 1×10^{49}. We include luminosity evolution in the form $L(z) = L(0) \times e^{cz}$ (where $c = 4.8$ is the evolution parameter). In this calculation we consider the emission as entirely beamed. The value for Γ is the same as in model A, while $\delta_{min} = 1$, and $\delta_{max} = 5.83$. The positive evolution (brighter objects in the past) tends to steepen the resulting log N–log S at low fluxes. The flattening is due to the effects of beaming. Positive evolution for BL Lacs has been ruled out (e.g., by Maccacaro et al. 1984a) on the assumption that the emission is isotropic. What we want to show here is that beaming can mimic the effect of "negative" evolution, even when a real "positive" evolution is present. The log N–log S slope at high fluxes is steeper than in the models previously assumed. The resulting log N–log S for this third model (C1, *solid line*) is shown in Figure 3*c*.

It is evident from Figure 3 that the three models are compatible, within the errors, with the observed number-counts, even if they differ, both in shape and in the underlying physics. Part of the problem lies in the fact that errors in the observed distribution are relatively large due to the relatively small number of objects detected and the small areas surveyed.

The models produce different redshift distribution. To further test their validity and/or constrain the range of their parameters, we can use the available redshift information. As part of a separate program, redshift measurements for a fraction of the EMSS BL Lac objects that constitute a complete subsample in the flux range 1×10^{-12} to 3×10^{-12} ergs cm^{-2} s^{-1} have been collected. We can then compare the observed redshift distribution with the different distributions predicted by the models. The distributions of redshifts predicted at 1×10^{-12} and 3×10^{-12} ergs cm^{-2} s^{-1} by the various models are not significantly different, so that the effect on the redshift distribution of the different areas surveyed at the two fluxes is negligible.

In Figure 4, one histogram for each of the models (A1, B1, C1) is plotted over the observed distribution of redshifts from the EMSS sources in the $1–3 \times 10^{-12}$ flux range. It is clear that the distribution of C1 is not compatible with the observed distribution, so we can reject this model as an explanation of the BL Lac XLF. That is, if beaming is the only effect involved, it is very unlikely that the AGN are the BL Lac parent population. This was also suggested by Schwartz and Ku (1983) on the basis of considerations about the relative volume densities. The other models (As and Bs) produce distributions that are not acceptable by a statistical test (the Kolmogorov-Smirnov test gives a probability of only 5×10^{-3} that the predicted and

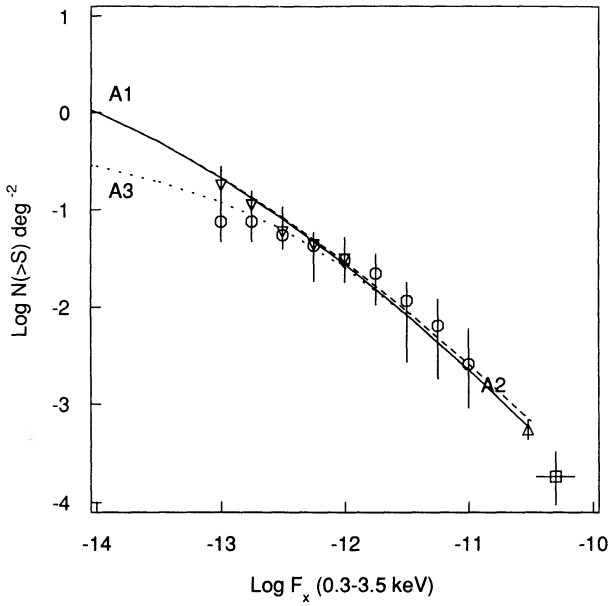

FIG. 3a

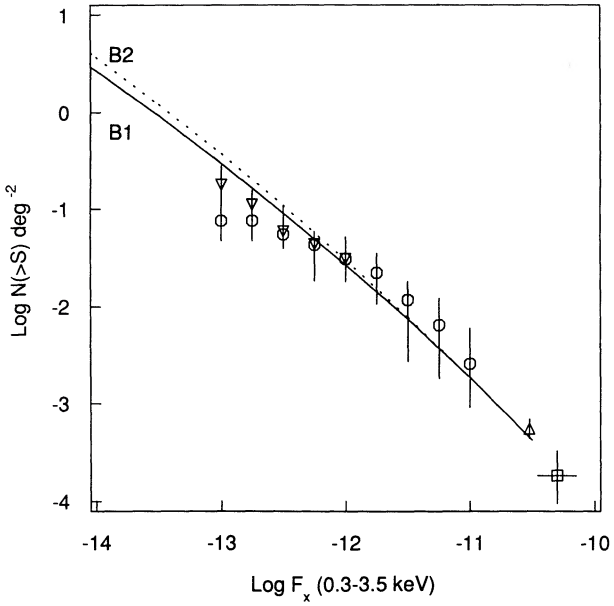

FIG. 3b

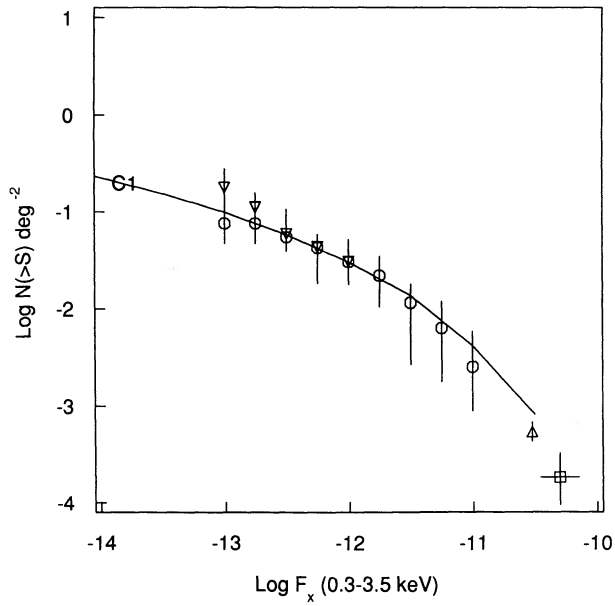

FIG. 3c

FIG. 3.—Data points are indicated as in Fig. 2. *EXOSAT* points are not repeated for graphical clarity since they are in the same flux range as EMSS points and consistent with them. The log $N(>S)$–log S relationships computed assuming different models are plotted: (*a*) model A1 (*solid line*), model A2 (*dashed line*), and model A3 (*dotted line*); (*b*) model B1 (*solid line*) and model B2 (*dotted line*); (*c*) model C1 (*solid line*).

observed distributions can be drawn from the same parent population). The big discrepancy for type B models is the large predicted number of $z < 0.15$ objects, while none is in fact observed. The number of BL Lac objects with redshift $z < 0.15$ predicted from the model B1, is ~ 6. The Poisson probability of finding no objects, when six are expected, is 3.5×10^{-3}. This discrepancy is remarkable especially because the nearest objects should be the easiest to observe; the galaxy should be more visible, so the absorption lines due to the stellar spectrum should be easier to detect. If this discrepancy is confirmed by further studies, then this model will need to be revised. An agreement was found in Padovani & Urry (1990) between the redshift distribution predicted by this model (at all fluxes greater than 2.5×10^{-13} ergs cm^{-2} s^{-1}) and a distribution of observed redshift. It is, however, important to recall that the redshifts in Padovani & Urry (1990) do not come from a complete sample, but from a composite sample taken at different fluxes. Since the redshift distribution for this model varies as a function of flux, an appropriate weight (on the area of sky observed at each flux) should be applied to the observed redshift distribution before comparing it with the predictions.

The predicted distributions of redshifts from the various models become even more different at lower fluxes. In Figure 5, the distributions in the range $1–3 \times 10^{-13}$ ergs cm^{-2} s^{-1}, for the same models as in Figure 4, are plotted. In the EMSS there are only two objects in this flux range, so a comparison is not possible on a statistical basis. However, an all-sky survey down to 1×10^{-13} ergs cm^{-2} s^{-1} like that carried out by *ROSAT* should find a large number of BL Lac objects (~ 1000), with almost 100 in the relevant flux range.

5. CONCLUSIONS

We presented the observed number-count relationship for X-ray–selected BL Lac objects. Surveys from different instruments are shown to agree with each other in measuring the surface density of BL Lac objects in the overlapping flux region. Log $N(>S)$–log S relationships were computed by integrating different models of X-ray luminosity functions and were compared with the observations. The flattening of the counts below 1×10^{-12} ergs cm^{-2} s^{-1} is now well established and described with enough accuracy. Beaming in the X-ray emission of BL Lac objects can reproduce this flattening in various cases. The number of redshifts available at present has been used to discriminate between different XLF models. In this way we have ruled out that the AGN XLF can reproduce the redshift distribution of BL Lac objects. Upon completion of the redshift measurements of the EMSS BL Lac objects, it

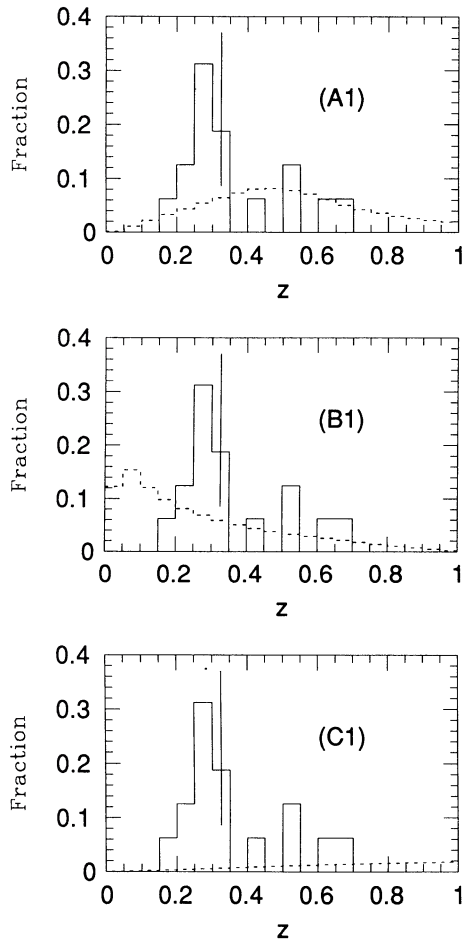

FIG. 4

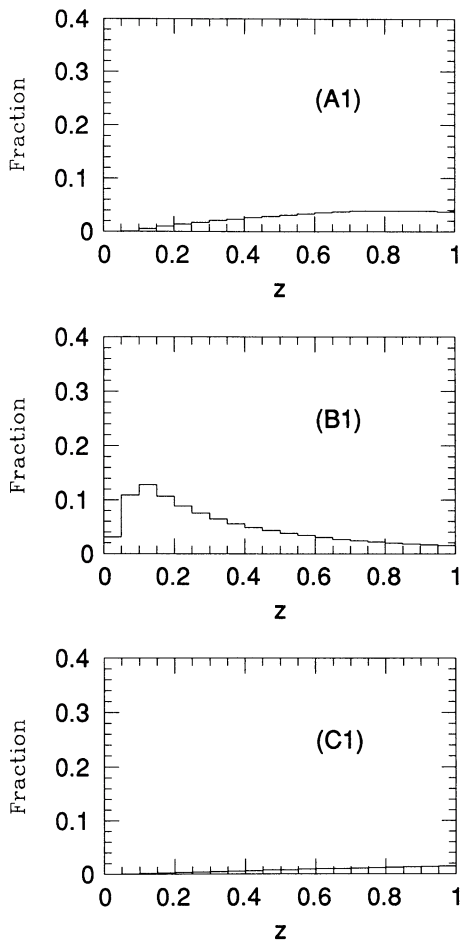

FIG. 5

FIG. 4.—Comparison of the observed redshift distribution (*solid line*) with the distribution predicted by the different models (*dashed lines*) in the flux range $1–3 \times 10^{-12}$ ergs cm^{-2} s^{-1}. The three panels correspond to models A1, B1, and C1 as described in the text. An indicative error bar is plotted to describe the present statistics.

FIG. 5.—The redshift distribution predicted by the same models as in Fig. 4 in the flux range $1–3 \times 10^{-13}$ ergs cm^{-2} s^{-1}

will be possible to discriminate among models that produce similar number-count relationships.

We thank Meg Urry for helpful suggestions and constructive criticisms, and Harvey Tananbaum and Dan Schwartz for many useful comments on an earlier version of this manuscript. This work has received partial financial support from NASA contract NAS8-30751, NASA grant NAG8-658, NSF grant AST-9715983, and from the Smithsonian Institution Scholarly Studies Program grant SS88-3-87.

REFERENCES

Cavaliere, A., Giallongo, E., & Vagnetti, F. 1986, A&A, 156, 33
Ghisellini, G., and Maraschi, L. 1989, ApJ, 340, 181
Gioia, I. M., Maccacaro, T., Schild, R. E., Wolter, A., Stocke, J. T., Morris, S. L., & Henry, J. P. 1990, ApJS, 72, 567
Giommi, P., et al. 1989, in Lecture Notes in Physics, 334, BL Lac Objects, ed. L. Maraschi, T. Maccacaro, & M.-H. Ulrich (Berlin: Springer), p. 231
Hewitt, A., & Burbidge, G. 1987, ApJS, 63, 1
Maccacaro, T., Gioia, I. M., Maccagni, D., & Stocke, J. T. 1984a, ApJ, 284, L23
Maccacaro, T., Gioia, I. M., Schild, R. E., Wolter, A., Morris, S. L., & Stocke, J. T. 1989, in Lecture Notes in Physics, 334, BL Lac Objects, ed. L Maraschi, T. Maccacari, & M.-H. Ulrich (Berlin: Springer), p. 222
Maccacaro, T., Gioia, I. M., & Stocke, J. T. 1984b, ApJ, 283, 486
Maccacaro, T., Gioia, I. M., Wolter, A., Zamorani, G., & Stocke, J. T. 1988, ApJ, 326, 680
Morris, S. L., Stocke, J. T., Gioia, I. M., Maccacaro, T., Schild, R. F., & Wolter, A. 1991, in preparation
Padovani, P., & Urry, C. M. 1990, preprint.
Piccinotti, G., Mushotzky, R. F., Boldt, E. A., Holt, S. S., Marshall, F. E., Serlemitsos, P. J., & Shafer, R. A. 1982, ApJ, 253, 485
Schwartz, D. A., & Ku, W. H.-M. 1983, ApJ, 266, 459
Schwartz, D. A., Brissenden, R. J. V., Tuohy, I. R., Feigelson, E. D., Hertz, P. L., & Remillard, R. A. 1989a, in Lecture Notes in Physics, 334, BL Lac Objects, ed. L. Maraschi, T. Maccacaro, & M.-H. Ulrich (Springer-Verlag), p. 209.
———. 1989b, BAAS, vol 22, No 2, p. 777
Stark, A. A., Heiles, C., Bally, J., & Limke, R. 1984, Bell Labs, privately distributed magnetic tape
Stocke, J. T., Morris, S. L., Gioia, I. M., Maccacaro, T., Schild, R. E., & Wolter, A. 1988, in Optical Surveys for Quasars, ed. P. S. Osmer, A. C. Porter, R. F. Green & C. B. Foltz (ASP Cmf. Ser., 2), p. 311
———. 1990a, ApJ, 348, 141
Stocke, J. T., Morris, S. L., Fleming, T., Gioia, I. M., Maccacaro, T., Schild, R. E., Wolter, A., & Henry, J. P. 1990b, ApJ, submitted
Urry, C. M., & Shafer, R. A. 1984, ApJ, 280, 569